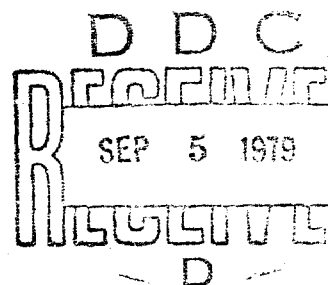ESD-TR-79-150

LEVEL

Technical Note	1979-35
Performance Limitations on Parameter Estimation of Closely Spaced Optical Targets Using Shot-Noise Detector Model	M-J. Tsai K-P. Dunn D D C RECEIVE SEP 5 1979 D 13 June 1979

Lincoln Laboratory

MASSACHUSETTS INSTITUTE OF TECHNOLOGY

LEXINGTON, MASSACHUSETTS

79 09 4 082

This technical report has been reviewed and is approved for publication.

FOR THE COMMANDER

Joseph C. Syiek
Project Officer
Lincoln Laboratory Project Office

LEVEL

MASSACHUSETTS INSTITUTE OF TECHNOLOGY

LINCOLN LABORATORY

PERFORMANCE LIMITATIONS ON PARAMETER ESTIMATION OF CLOSELY SPACED OPTICAL TARGETS USING SHOT-NOISE DETECTOR MODEL
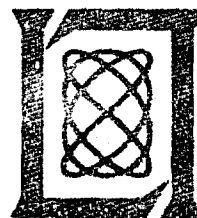
M-J. TSAI
K-P. DUNN

Group 32

TECHNICAL NOTE 1979-35

13 JUNE 1979

D D C

SEP 5 1979

LEXINGTON   MASSACHUSETTS

ABSTRACT

A mathematical model for passive optical sensors, which takes into account the inherent shot-noise process, is presented. Based on this sensor model, the Cramer-Rao bounds on the variances of intensity and angular location estimates for two closely spaced optical targets are derived. Representative results for the estimation performance degradation due to the interfering targets are shown.

iii

CONTENTS

I. INTRODUCTION

Resolving closely spaced objects (CSO) has been a serious problem for radar and optical sensor systems [1]-[3]. Recent attention has concentrated on the problem of determining accurately both target amplitude and location for situations in which the target density is high. Techniques that are applicable to predicting the performance of amplitude and position estimators for both radar and optical systems have been described and compared [4]. The Cramer-Rao lower bounds on the variance of target amplitude and location estimates are well-known to radar system designers, and they have proved useful in predicting the performance limitation of sensor systems without the need for extensive simulations or experiments. In references [4] and [5], the Cramer-Rao lower bounds on the performance of target amplitude and location estimates have been derived for closely spaced opitcal targets. Theoretical bounds presented in [3] are obtained using a different error analysis technique and, furthermore, the parameters to be estimated are different from those considered in [4] and [5]. The noise model assumed in these reports was white gaussian noise, which applics only to the background noise limited case. Various pulse shapes have been considered. Some of them were rather simple shapes typical of radar pulses, see for example [4]. A particular pulse shape which approximates to the pulse shape in [3] also considered in [4]. A gaussian function approximation

1

to the optical diffraction pattern was used in [5] to obtain the
pulse shape at the detector output for an optical point target.

In this report we reformulate the problem introducing a more
general noise environment and a more realistic optical pulse shape.
In the next section, we present the mathematical model of the optical
system involved in the detection and estimation problem. Special
consideration is given to the model of optical sensors. In Section
III a temporal optical signal produced by a scanning detector is
described. The applicaiton of this detector model and pulse shape
to the estimation problems for closely spaced optical targets is
presented in Section IV. Some numerical results are also included
in this report. These results emphasize but are not restricted to
the detector noise limited case.

II. THE MODEL OF OPTICAL DETECTING SYSTEM

A typical optical receiving system consists of three basic
blocks: an optical receiving lens system, a photodetector, and
a postdetection processor, as shown in Fig. 1. The lens system
collects the incident optical field radiated from remote sources
(or targets) as well as background noises. This received
optical field is focused and filtered by the receiving lens system
onto the photodetector surface and then converted to an electrical
signal by the photodetector. This conversion process is quite
complicated and it can not be modelled as a deterministic process,
because the photodetector responds to the impinging radiation
field by releasing electrons from its surface at random. This
intrinsic fluctuation is often modelled as a shot noise process, a
more detailed description of this process will be given in the next
sub-section. Other noise sources in the receiving system are:
the circuit and electronic noise generated in the signal processing
operations which is often referred to as the thermal noise, and the
"dark current" in the photodetector corresponding to the random
emisson of electrons at a fixed rate when no incident field is
present. The processor performs the necessary amplification and
filtering (electronically) operations to recover the desired in-
formation from the noisy photodetector output. In this section we
will concentrate on the model of the photodetector system.
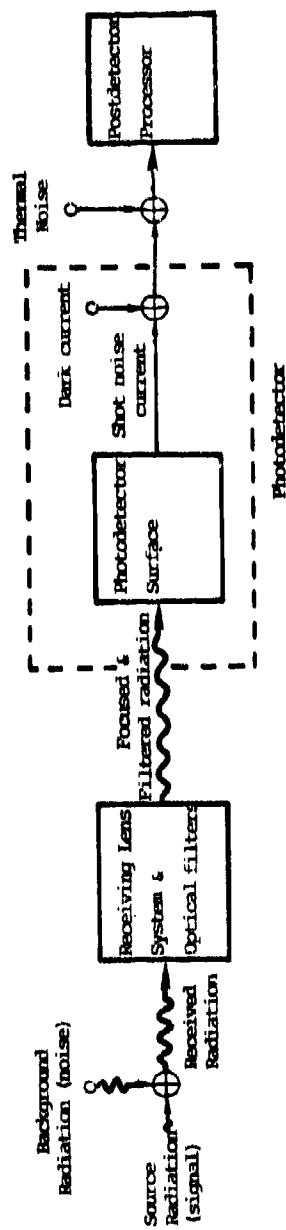
Fig.1. The optical receiving system.

4

2.1   The Photodetector Response Process

2.1.1   Shot Noise Process

A photoemissive photodetector has the basic structure shown in Fig. 2. The photosensitive surface responds to the impinging radiation by releasing electrons randomly at a rate determined by the incident intensity. These free electrons are collected by a collecting anode due to the applied electric field. The current induced by these moving electrons can be represented by the following mathematical expression

$$x(t) = \sum_{j=1}^{N(0,t)} h(t-t_j), \qquad (2.1)$$

where $h(t)$ is the current response function corresponding to the movement of a single electron from the photosensitive surface to the collecting anode, t_j is the instant that the jth electron is released from the surface, and $N(0,t)$ is the number of electrons released from the surface over the interval $(0,t)$.

In all cases, the area under the response function is a fixed constant, since the integral of $h(t)$ is the charge of a single electron, that is

$$\int_0^\infty h(t)\,dt = \text{charge of a single electron} \triangleq e. \qquad (2.2)$$

Although the current response function may be different for each individual electron, for simplicity we assume that every electron has the same response function $h(t)$. Since the travel time of each

Photosensitive
Surface

Current

Released
Electrons

Received
Field

Collecting
Anode

R_L

Voltage
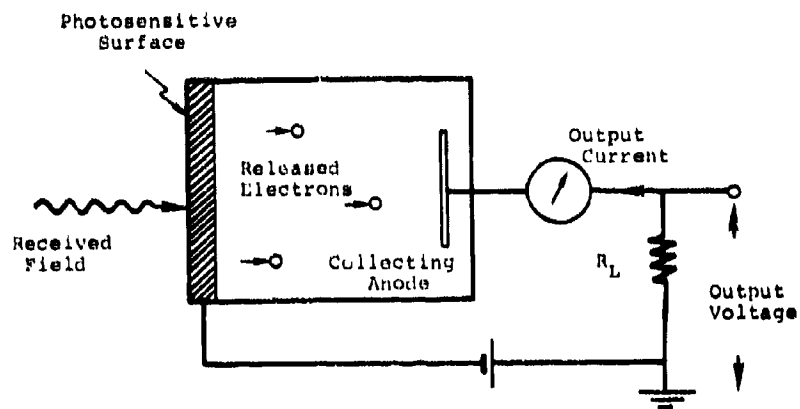
Fig.2.   Photodetector model.

electron is finite, the function h(t) must be time limited to some interval τ_h. That is, h(t) = 0 for t<0 and t>τ_h. This time interval τ_h is inversely related to the detector bandwidth and it is relatively short (10^{-7} to 10^{-9} sec.) compared with the time variations of the signals considered in this report. For simplicity, we may assume that

$$h(t) = \begin{cases} \dfrac{e}{\tau_h} & 0<t<\tau_h \\ \\ 0 & \text{otherwise.} \end{cases} \tag{2.3}$$

Substituting this back to (2.1), we have

$$x(t) = \frac{e}{\tau_h} \, N(t-\tau_h, t). \tag{2.4}$$

N(0,t), often referred as a counting process, is actually a Poisson process whose intensity, n(t), is proportional to the power received by the detector [6], [7]. In many cases, n(t) is itself a random process and hence N(0,t) becomes a conditional Poisson process. x(t), the current at the detector output is known as a shot noise or conditional shot noise process depending on whether n(t) is deterministic or random. More detailed descriptions of these processes and their statistical properties can be found in [6]-[8]. In the following we will give the mean and covariance functions of the resulting conditional Poisson shot noise, x(t), without derivation:

$$E[x(t)] = \int_{-\infty}^{t} h(t-z) \; E[n(z)] dz \tag{2.5}$$

7

$$\text{Cov}_x(t, t+\tau) = \int_{-\infty}^{t} h(t-z) h(t+\tau-z) \, E[n(z)] \, dz. \qquad (2.6)$$

If the current response function of the photodetector, h(t), is given by (2.3) and its bandwidth $(1/\tau_h)$ is much larger than that of n(t), then we have the following approximations

$$E[x(t)] = eE[n(t)] \qquad (2.5a)$$

and

$$\text{Cov}_x(t, t+\tau) \cong \begin{cases} \left(\dfrac{e}{\tau_h}\right)^2 (\tau+\tau_h) E[n(t)] & -\tau_h < \tau \leq 0 \\[2ex] \left(\dfrac{e}{\tau_h}\right)^2 (\tau_h-\tau) E[n(t)] & 0 \leq \tau < \tau_h \\[2ex] 0 & \text{otherwise} \end{cases} \qquad (2.6a)$$

Note that the dependence on t in (2.5) and (2.6) indicates that the general detector process, x(t), is nonstationary.

2.1.2 Intensity Process

The intensity of the shot noise process of a photodetector output is a function of the incident field power and other factors related to the photosensitive material used. A simplified mathematical model is used in this report as well as other references [6] - [8]. The intensity, n(t), of the shot noise process (also referred to as count energy, or count power, for example, in reference [6]) is linearly proportional to the received field power,

8

P(t), at time t

$$n(t) = \rho \, P(t), \tag{2.7}$$

where

$$\rho = \frac{\eta}{hf} \tag{2.8}$$

and

      η: Quantum efficiency

      h: Planck's constant

      f: Optical frequency.

If the incident field involves certain random sources, for example background noises, then the intensity is no longer deterministic. In most cases considered here, the resulting shot noise process is a conditional Poisson shot noise process.

2.1.3   Background Noise

There are two basic types of background noise sources which may appear in the field of view of the photodetector, they are: (1) the diffuse sky background, which is assumed uniformly radiant over the whole hemisphere, and therefore is always in the field of view of the detector, and (2) discrete, or point, sources such as stars, planets, sun and the like, that are more localized but more intense, and may or may not be in the field of view of the detector. In this report we will only consider the uniform background radiation noise.

A common model for this uniform background radiation is to

9

assume the sky appears as an ideal blackbody radiator. Then the average background noise power collected on the detector surface is

$$P_b = N_{ob} B_o \frac{\Omega_{fv}}{\Omega_{dL}} \qquad (2.9)$$

where Ω_{fv} is the detector field of view, Ω_{dL} the diffraction limited field of view of the lens system, B_o the optical filter bandwidth and N_{ob} the effective spectral level for a blackbody radiator at temperature T degrees Kelvin:

$$N_{ob} = \frac{hf}{e^{hf/kT} - 1} \qquad (2.10)$$

where k is Boltzmann's constant.

2.1.4 Gaussian Approximation for the Shot Noise Process

If the intensity, n(t), is significantly "large", the instantaneous probability density of the shot noise process can be approximated by the probability density of a Gaussian process with mean and covariance given by (2.5) and (2.6), respectively. A rigorious justification of this can be found in [7].

2.1.5 Dark Current and Thermal Noise

Dark current in a photodetector corresponds to the random emission of electrons at a fixed rate, when no field is being detected. This current is added directly to the shot-noise current

10

at the detector output. In typical operation, the average level of the dark current is much less than the average level of the shot-noise current and the dark current can often be neglected.

Thermal noise is always present in an electrical element. Its magnitude depends on the temperature of the element and the bandwidth of the processing filter which the element feeds. This thermal noise in an optical system is often considered as an additive gaussian noise to the shot noise. However, its effect can be usually made negligible by operating the detector in a very low temperature environment (semiconductor type) or with a very high current gain (photomultiplier type).

2.2   Signal-to-Noise Ratio

Let $s(t)$ and P_b be the average signal and background noise power received by the photodetector. Then the average count intensity is, from (2.7),

$$E[n(t)] = \rho(s(t)+P_b) \ . \tag{2.11}$$

According to (2.5a) and (2.6a), the mean of the shot noise process is

$$E[x(t)] = e\rho(s(t)+P_b) \tag{2.12}$$

and the variance

$$\text{Var}[x(t)] = \frac{e^2\rho}{\tau_h} (s(t)+P_b) \ . \tag{2.13}$$

11

It is clear that the shot noise process is not simply a desired signal plus an additive noise. Instead, the desired signal is immersed in the noise. The conventional definition of instantaneous signal-to-noise ratio (SNR_t) for this particular case is [6]

$$SNR_t \triangleq \frac{[\text{mean of the shot noise due to s(t) at time t}]^2}{\text{shot noise variance at time t}}. \quad (2.14)$$

Suppose, in the post-detection processor, the constant mean ($e^2 \rho P_b$) of the shot noise due to uniform background radiation is removed and the remainder of x(t) is filtered by a low pass filter with unit gain and bandwidth B. In general, this bandwidth must be selected such that it is much smaller than the bandwidth of the detector current response function ($1/\tau_h$) and much larger than the bandwidth of the s(t). At the filter output, the mean signal is equal to $e\rho s(t)$ and the variance of noise is equal to $[e^2 \rho (s(t)+P_b)+N_{oc}]2B$ where N_{oc} is the two-sided power spectral density of the thermal current noise. Therefore, SNR_t becomes

$$SNR_t = \frac{e^2 \rho^2 s^2(t)}{[e^2 \rho (s(t)+P_b)+N_{oc}]2B}. \quad (2.15)$$

If $e^2 \rho (s(t)+P_b) >> N_{oc}$, that is, if the noise current contributed by the shot noise process greatly exceeds the thermal noise current, the second term in the denominator can be dropped, and we say the receiver is shot noise limited. That is,

$$SNR_t = \frac{\rho s^2(t)}{(s(t)+P_b)2B}. \quad (2.16)$$

12

Substituting for ρ by (2.8), we have

$$SNR_t = \frac{\eta s^2(t)}{2hfB(s(t)+P_b)} \quad . \qquad (2.16a)$$

It is important to note that the signal-to-noise ratio does not
increase without bound as the background noise (P_b) and circuit noise
(N_{oc}) are weakened, but rather approaches the following limit:

$$SNR_t = \frac{\eta s(t)}{2hfB} \quad . \qquad (2.17)$$

In this case, we say the receiver is <u>quantum limited</u>. This is a
major difference between an optical receiving system and its
microwave counterpart. At the other extreme, the background noise
power greatly exceeds the signal power and we have a <u>background
limited condition</u>. In this case, (2.16a) becomes

$$SNR_t = \frac{\eta s^2(t)}{2hfBP_b} \quad . \qquad (2.18)$$

Since the output noise is dominated by the background noise
in this background limited case, one may describe the signal and
noise relation by the usual "signal plus noise" concept (where
the noise covariance is independent of the signal) which is
familiar to communication engineers. However, in general, this
interpretation of signal and noise relationship may lead to
incorrect conclusions.

13

III. OPTICAL PULSE SHAPES

The radiation emitted from a remote point target forms an image in the focal plane of a telescope. A detector is often used to scan through the image and thus it receives a time-varying optical signal associated with the fixed image. This optical signal together with the background noise appears on the detector photosensitive surface and produces a shot-noise current at the detector output. The pulse shape of the time-varying optical signal is considered in this section

Let us first assume the incident optical field from the remote point target is monochromatic (wavelength λ) and normal to the aperture at its center, and that the aperture lens is aberration-free and rectangular with dimension (d,b). Then according to the Fraunhofer transformation [9] the diffracted field intensity in the focal plane is

$$s_f(x,y) = \frac{EA}{\lambda^2 f_c{}^2} \left(\frac{\sin\left(\pi dx/(\lambda f_c)\right)}{\pi dx/(\lambda f_c)}\right)^2 \left(\frac{\sin\left(\pi by/(\lambda f_c)\right)}{\pi by/(\lambda f_c)}\right)^2 \quad (3.1)$$

where E is the total energy collected by the lens, which is proportional to the intensity of the point source and inversely proprotional to the square of the distance from the point source to the telescope, f_c the focal length, A = db the aperture area and (x,y) the rectangular coordinates in the focal plane. Next we assume the detector is rectangular with dimensions w_1 and w_2 in the x and y directions, respectively, and has response function given by

14

$$g(x,y) = \begin{cases} 1 & |x| \leq \frac{w_1}{2} \text{ and } |y| \leq \frac{w_2}{2} \\ 0 & \text{otherwise.} \end{cases} \qquad (3.2)$$

The input of the detector after the scanning process (i.e., the incident signal power at the photosensitive surface) is then given as the convolution integral of $g(x,y)$ and $s_f(x,y)$,

$$s_d(x_o,y_o) = \int_{-\infty}^{\infty} \int_{-\infty}^{\infty} s_f(x,y)\ g(x_o-x,\ y_o-y)dxdy \qquad (3.3)$$

where (x_o,y_o) is the center position of the detector.

The scanning process converts the spatial structure of the image into a temporal signal. If the scanning rate is fixed, the resultant temporal signal function will have the same form as the image spatial function. Here we further assume that the detector scans along the x-axis with a constant scan rate, v_x. This simply means

$$x_o = v_x t, \qquad (3.4)$$

and

$$y_o = 0. \qquad (3.5)$$

Substituting (3.1), (3.2), (3.4) and (3.5) into (3.3) and carrying out the integral we can write the temporal optical signal at the detector as

$$s_d(t) = a\ s_o(t) \qquad (3.6)$$

where

15

$$a = \frac{E}{\pi^2} \int_{k_1}^{k_2} \frac{\sin^2 v}{v^2} \, dv \qquad (3.7)$$

and

$$s_0(t) = Si(2\pi\alpha t+\pi\beta) - \frac{\sin^2(\pi\alpha t+\pi\beta/2)}{\pi\alpha t+\pi\beta/2}$$

$$- Si(2\pi\alpha t-\pi\beta) + \frac{\sin^2(\pi\alpha t-\pi\beta/2)}{\pi\alpha t-\pi\beta/2} . \qquad (3.8)$$

Here, $Si(x)$ is the sine integral evaluated at x. The constants which appear in Equations (3.7) and (3.8) are as follows

$$k_1 = \frac{\pi(y_0-w_2/2)}{f_c(\lambda/b)} ,$$

$$k_2 = \frac{\pi(y_0+w_2/2)}{f_c(\lambda/b)} ,$$

$\alpha = (v_x/f_c)/(\lambda/d)$, (normalized angular scanning rate)

$\beta = (w_1/f_c)/(\lambda/d)$. (normalized detector angular width)

If w_2 is significantly larger than the extent of the point source image formed by the telescope, then a in (3.7) can be approximated by E/π.

When there are n incoherent point sources located at angles $\Theta_1,\ldots,\Theta_n$ along the x-axis, the resulting optical signal at the detector is simply the superposition of response from each target;

$$s_d(t) = \sum_{i=1}^{n} a_i s_0(t-\tau_i) \qquad (3.9)$$

16

where

$$\tau_i = \frac{O_i}{v_x/f_c} .$$ (3.10)

Note that the time frequency, f, of the optical signal is related to the spatial frequency, f_s, by

$$f = f_s \cdot v_x$$ (3.11)

Usually v_x should be high enough to avoid problems with target motion during detection on one hand and should be as low as possible to ease the subsequent signal processing on the other hand.

In deriving (3.6) - (3.10) we have made several assumptions. The diffraction pattern under these assumptions is of the form $(\sin \mu/\mu)^2$. When any one of these assumptions is modified the shape of the diffraction pattern would be different.* For example, if the aperture lens area is circular the diffraction pattern is given by $(2J_1(\mu)/\mu)^2$ where $J_1(\mu)$ is the Bessel function of the first kind [9]. If the incident optical field has finite bandwidth instead of being monochromatic and telescope aberration is unavoidable, the diffraction pattern might be better approximated with a gaussian function of the form [10]

$$s_f(x,y) = \frac{E}{2\pi\sigma^2} \text{Exp} - \left(\frac{x^2+y^2}{2\sigma^2}\right)$$ (3.12)

where σ depends upon the spectral bandwidth of the incident radiation and the aberration of the telescope.

---

*Pulse shapes different from $s_o(t)$ given in (3.8), are easily incorporated into the analysis described in the following sections.

17

IV.   PERFORMANCE LOWER BOUNDS FOR INTENSITY AND LOCATION ESTIMATES

In many optical sensor applications, it is necessary to estimate
the target intensity and angular location from the signal collected
at the output of a post-detection filter or a detector itself. It
is expected that the quality of the estimates for a desired target
degrades when there are interfering targets. In [4] and [5], the
Cramer-Rao lower bounds on the variances of these estimates were used
to characterize the degraded performance. These bounds are frequently
easy to calculate and are generally tight bounds for a wide class of
unbiased estimators when the signal-to-noise ratio is high (see for
example, [11]-[14]). In general, these bounds shall not be inter-
preted as the achievable performances but rather the lower bounds
on the achievable performances of unbiased estimators. In the
following subsection, we will first derive the Cramer-Rao bounds
(CRB's) associated with the sensor and signal (optical pulse shape)
models described in the previous sections. Secondly the so-called
"degradation factor" - the ratio of CRB with interfering target
and CRB without interfering target will be derived.

4.1   Cramer-Rao Lower Bounds

Suppose $\underline{y} = \{y, \ldots, y_k\}$ is a sequence of observations and
$\underline{\omega} = \{\omega_1, \omega_2, \ldots, \omega_q\}$ is a set of parameters to be estimated. Then
the CRB on the unbiased estimators for $\underline{\omega}$ given the observations
$\underline{y}$ is obtained by inverting the Fisher information matrix with its

18

$(i,j)^{th}$ element defined by [11]

$$F_{ij} = E \left\{ \left(\frac{\partial \log p(\underline{y}/\underline{\omega})}{\partial \omega_i} \right) \left(\frac{\partial \log p(\underline{y}/\underline{\omega})}{\partial \omega_j} \right) \right\} \qquad (4.1)$$

where $E \{ \}$ denotes statistical expectation, ω_i the ith element of the unknown parameter vector, $\underline{\omega}$, and $p(\underline{y}/\underline{\omega})$ the joint probability density function of $\underline{y}$ given $\underline{\omega}$.

From discussions in Section II, we know that the current at the detector output, $x(t)$, is a Poisson shot noise process as described by (2.1). $x(t)$ is always contaminated by the thermal noise which is usually modeled as additive gaussian noise. However we intend to omit this type of noise because it is practically negligible in most applications. We also know that the count intensity, $n(t)$, of the shot noise process is proportional to the received optical power which is the sum of the background radiation power, P_b, and the signal power $s_d(t)$. That is

$$n(t) = \rho(s_d(t)+P_b), \qquad (4.2)$$

where P_b is given in (2.9) and $s_d(t)$ is given in (3.9).

Suppose an ideal integrator is used as the post-detection filter. The integrator integrates and resets every τ_p seconds during $(-T/2, T/2)$. A sequence of measurements on the integrator output current, $\underline{y} = (y_1, \dots, y_k)$ is obtained at $t_\ell = -\frac{T}{2} + \ell \tau_p$, $\ell = 1, \dots, k$. Suppose $\tau_p \gg \tau_h$ and $\tau_p \approx 1/(2B_n)$ where τ_h is the duration of the detector impulse response as described previously and B_n is

19

the bandwidth of the count intensity, $n(t)$. Then we have

$$y_\ell = \frac{e}{\tau_p} N(t_\ell - \tau_p, t_\ell)$$

$$= \frac{e}{\tau_p} N(t_{\ell-1}, t_\ell) \qquad (4.3)$$

which is similar to $x(t_\ell)$ in (2.4) except τ_h is replaced by τ_p.
The electron counts $N_\ell = N(t_{\ell-1}, t_\ell)$, $\ell=1,\ldots,k$ are independent
and Poisson distributed when conditioned on the count intensity,
$n(t)$. The unknown parameters, $\underline{\omega}$, which we wish to estimate from
the observations $\underline{y}$ are the intensities and angular locations of the
n targets appeared in the field of view of the detector, namely,
a_i's and τ_i's of Eq. (3.9). Therefore, we may define

$$\begin{cases} \omega_i = a_i \\ \omega_{n+i} = \tau_i \end{cases} \qquad (4.4)$$

for $i=1,\ldots,n$.

In order to compute the Fisher information matrix according to
(4.1), we need the joint conditional probability density function
$p(\underline{y}/\underline{\omega})$. From Eq. (4.3) and the fact that $N_\ell, \ell=1,\ldots,k$ are mutually
independent, we have

$$p(\underline{y}/\underline{\omega}) = \prod_{\ell=1}^{k} P(N_\ell = \frac{y_\ell \tau_p}{e} /\underline{\omega})$$

$$= \prod_{\ell=1}^{k} \frac{(m_\ell)^{N_\ell}}{N_\ell !} \exp\{-m_\ell\} \qquad (4.5)$$

where

$$m_\ell = \text{mean (or variance) of } N_\ell$$

$$= \int_{t_{\ell-1}}^{t_\ell} n(t)\, dt$$

$$\cong \rho\tau_p \,[s_d(t_\ell)+P_b] \tag{4.6}$$

It is easy to obtain that [3]

$$F_{ij} = \sum_{\ell=1}^{k} \frac{\rho\tau_p}{s_d(t)+P_b} \; \frac{\partial\, s_d(t_\ell)}{\partial\, \omega_i} \; \frac{\partial\, s_d(t_\ell)}{\partial\, \omega_j} \tag{4.7,}$$

where

$$\frac{\partial\, s_d(t)}{\partial\, \omega_i} = \begin{cases} s_o(t-\tau_j) & \text{if } \omega_i = a_j \\[2mm] -a_j \dot{s}_o(t-\tau_j) & \text{if } \omega_i = \tau_j. \end{cases} \tag{4.8}$$

The Cramer-Rao lower bound for each component of the unknown parameter $\underline{\omega}$ can be calculated easily by inverting the Fisher information matrix F, that is

$$\sigma_{\omega_i}^2 \geq (F^{-1})_{ii}. \tag{4.9}$$

This result is applicable to the shot-noise limited case. If the condition for the background limited case is satisfied, i.e.,

21

$s_d(t) << P_b$, then we can further reduce (4.7) to

$$F_{ij} = \frac{\rho \tau_p}{P_b} \sum_{\ell=1}^{k} \frac{\partial s_d(t_\ell)}{\partial \omega_i} \frac{\partial s_d(t_\ell)}{\partial \omega_j} \tag{4.10}$$

Notice that this formula is a discrete counterpart of the Cramer-Rao bound obtained in [4]. More detailed discussion about the comparison between our results and results in [4] will be given in a future report.

In deriving (4.7)-(4.10), the current gain of the detector is assumed equal to unity. However this assumption is made only for convenience of analysis. It can be easily shown that the same equations can be obtained for different current gain as long as it is a constant.

It was pointed out previously that the optical detector shot-noise process can be approximated by a gaussian process when the count intensity $n(t)$ is large. It can be shown that, based on the gaussian process, the same formula for the Fisher information matrix as given in (4.7) and (4.10) can be obtained if $n(t) >> 1/\tau_p$.

The unit-amplitude optical signal $s_o(t)$ and its derivative $\dot{s}_o(t)$ must be available in order to compute the Fisher information matrix in accordance with (4.7) or (4.10). Suppose $s_o(t)$ is given by (3.8). Then the necessary $\dot{s}_o(t)$ is given as

$$\dot{s}_o(t) = \left[\frac{\sin(\pi \alpha t + \pi \beta/2)}{\pi \alpha t + \pi \beta/2} \right]^2 - \left[\frac{\sin(\pi \alpha t - \pi \beta/2)}{\pi \alpha t - \pi \beta/2} \right]^2 \tag{4.11}$$

22

Both $s_o(t)$ and $\dot{s}_o(t)$ are dependent only on the normalized detector size β if the scanning rate α is kept constant.

In presenting results, it is convenient to rewrite (2.9) as below

$$P_b = P_{bo}\,\beta \tag{4.12}$$

where

$$P_{bo} = N_{ob}\omega_o\,\beta'$$

and $\beta' = (w_2/f_c)/(\lambda/b)$ is the normalized angular width of the detector in the direction perpendicular to the scanning direction. Since P_{bo} is independent of the scanning process, it is convenient to use it to normalize the signal, $s_d(t)$, that is

$$\tilde{s}_d(t) \stackrel{\triangle}{=} \frac{1}{P_{bo}}\,s_d(t)$$

$$= \sum_{i=1}^{n} \tilde{a}_i s_o(t-\tau_i). \tag{4.13}$$

Here $\tilde{s}_d(t)$ and $\tilde{a}_i$ denote the relative magnitudes of $s_d(t)$ and a_i with respect to P_{bo}, respectively. The $(i,j)^{th}$ element of the Fisher information matrix for the normalized unknown parameter becomes

$$\tilde{F}_{ij} = \sum_{\ell=1}^{k} \frac{N_a}{\tilde{s}_d(t_\ell)+\beta}\,\frac{\partial\,\tilde{s}_d(t_\ell)}{\partial\,\omega_i}\,\frac{\partial\,\tilde{s}_d(t_\ell)}{\partial\,\omega_j} \tag{4.14}$$

where

$$N_e = \rho \tau_p P_{bo} \qquad (4.15)$$

which is the average number of electrons released from a detector of angular width equal to λ/d (or $\beta=1$) due to background noise during the integration interval, τ_p. For the background-noise limited case or, equivalently, $\tilde{s}_d(t) \ll \beta$, Eq. (4.10) becomes

$$\tilde{F}_{ij} = \frac{N_e}{\beta} \sum_{\ell=1}^{k} \frac{\partial \tilde{s}_d(t_\ell)}{\partial \omega_i} \frac{\partial \tilde{s}_d(t_\ell)}{\partial \omega_j} . \qquad (4.16)$$

The expression of $\partial \tilde{s}_d(t_\ell)/\partial \omega_i$ is the same as $\partial s_d(t_\ell)/\partial \omega_i$ in (4.8) and (4.10) expect all a_i's should be replaced by $\tilde{a}_i$'s. It should be noted that for a observation interval, T, it can be easily seen that an increase of the integration interval, τ_p, will decrease the number of samples, k, but the value of F_{ij} will be unchanged.

The CRB's on the variances of intensity and position estimates are expected to be closely related to the signal-to-noise ratio To demonstrate this point let us consider, for simplicity, the single target and background noise limited case. Using (2.18) we can write for this case the instantaneous signal-to-noise ratio as

$$SNR_t = \frac{\rho s_d^2(t)}{P_b/\tau_p} \qquad (4.17)$$

or

$$SNR_t = \frac{N_e \tilde{a}_1^2}{\beta} s_o^2(t). \qquad (4.18)$$

Here, the target is assumed located at $\tau_1=0$. Obviously the SNR_t

is proportional to $N_e \tilde{a}_1^2/\beta$ for a fixed β. From (4.16), we have the associated Fisher information matrix,

$$\tilde{F} = \frac{N_e}{\beta}\begin{bmatrix} \sum s_o^2(t_\ell) & -\tilde{a}_1 \sum \dot{s}_o(t_\ell) s_o(t_\ell) \\ -\tilde{a}_1 \sum s_o(t_\ell) \dot{s}_o(t_\ell) & \tilde{a}_1^2 \sum \dot{s}_o^2(t_\ell) \end{bmatrix} \qquad (4.19)$$

since the off-diagonal entries of matrix F are relatively small (it can be shown that $s_o(t)$ and $\dot{s}_o(t)$ are orthogonal), it follows that

$$E\left[(\hat{\tau}_1-\tau_1)^2\right] \geq CRB(\tau_1,n=1) = \frac{\beta}{N_e\tilde{a}_1^2} \times \frac{1}{\sum \dot{s}_o^2(t_\ell)} \qquad (4.20)$$

and

$$\frac{E[(\hat{a}_1-\tilde{a}_1)^2]}{\tilde{a}_1^2} \geq \frac{CRB(\tilde{a}_1,n=1)}{\tilde{a}_1^2} = \frac{\beta}{N_e\tilde{a}_1^2} \times \frac{1}{\sum s_o^2(t_\ell)}. \qquad (4.21)$$

Here $\hat{\tau}_1$ and $\hat{a}_1$ denote the estimates of τ_1 and $\tilde{a}_1$; $CRB(\omega,n)$ denotes the Cramer-Rao bound of the estimate for parameter ω in the case of n targets. This implies that for a fixed value of β the CRB for the τ estimate and the normalized CRB for the $\tilde{a}$ estimate of a single target are inversely proportional to SNR in the background-noise limited case.

In other cases, CRB and SNR might be related in a more complicated manner. The reasons for this are twofold. First, in cases other than background limited, the noise is dependent upon the signal and

25

SNR_t is no longer simply proportional to $N_e \tilde{a}_1^2/\beta$. Secondly, in the presence of a second target, the signal due to this target becomes interference to the desired target. For the case of two targets (i.e., n=2 in (3.9)), the instantaneous signal-to-noise ratio for the 1st target can be obtained by modifying (2.14) as follows

$$SNR_t^1 = \frac{[m_1(t)]^2}{\text{variance of shot noise at time } t + [m_2(t)]^2} \qquad (4.22)$$

where $m_i(t)$ is the mean of shot noise due to the ith target, i=1 and 2. The interference from the second target becomes part of the total noise. The above equation can be expressed as

$$SNR_t^1 = \frac{[e\rho a_1 s_o(t-\tau_1)]^2}{\frac{1}{\tau_p}[e^2\rho(s_d(t)+P_b)] + [e\rho a_2 s_o(t-\tau_2)]^2} \qquad (4.23)$$

or equivalently,

$$SNR_t^1 = \frac{N_e \tilde{a}_1^2 s_o^2(t-\tau_1)}{(\tilde{s}_d(t)+\beta) + N_e \tilde{a}_2^2 s_o^2(t-\tau_2)} . \qquad (4.24)$$

Usually, the SNR_t^1 is specified at $t=\tau_1$ when the signal due to the 1st target is at its maximum.

4.2 Degradation Factors

In this report we are concerned with two cases; one is the case where there exists one target without any interference (n=1)

and the other is the case where there is an interfering target in addition to the desired target (n=2). Without loss of generality we can assume the target is at $\tau_1=0$ for the n=1 case and the two targets are at $\tau_1=-\Delta\tau/2$ and $\tau_2=\Delta\tau/2$ where $\Delta\tau=\Delta\Theta/(v_x/f_c)$ is the angular separation in terms of time. The subcripts 1 and 2 are used to indicate the first (desired) and the second (interfering) targets respectively.

The effect of an interfering target on the accuracy of intensity and angular position estimates of the desired target is customarily indicated by the so-called "degradation factor" which is defined as the square-root of the ratio of the CRB for the intensity (or angular position) estimate of the desired target in the presence of an interfering target to the CRB for the intensity (or angular position) estimate of the desired target without any interference. Mathematically, with DF_a and DF_τ denoting the degradation factors for intensity and position estimates, they are

$$DF_a = \left[\frac{CRB(\tilde{a}_1, n=2)}{CRB(\tilde{a}_1, n=1)}\right]^{\frac{1}{2}} \qquad (4.25)$$

$$DF_\tau = \left[\frac{CRB(\tau_1, n=2)}{CRB(\tau_1, n=1)}\right]^{\frac{1}{2}}. \qquad (4.26)$$

It is convenient to characterize the effect of interference by

these "degradation factors", if one is only interested in the change
of "relative" performance due to the interfering target. The optical
sensor noise models used in [4], [5] and the typical noise model
used for radar analysis assume an additive white gaussian noise.
In these cases the degradation factors are, generally, independent
of the signal-to-noise ratio of each target. To calculate the actual
estimation performance for a target with interference via the de-
gradation factor, in these cases, it is necessary to determine the
"absolute" performance of the desired target without interference.
It should be noted here that the degradation factors presented in
this report, except those for the background-noise limited cases,
are dependent upon several signal-to-noise ratio related parameters
such as normalized detector size (β), normalized target intensities
($\tilde{a}_1$ and $\tilde{a}_2$). The simple and universal representations of interference
effects via the degradation factors appropriate to the additive
white gaussian noise cases no longer apply here. These points
will be made clear when we examine the results presented in the next
section.

V. RESULTS

Previously, we discussed the mathematical model of optical
detectors, the nature of noise contributions, the pulse shape of a
point target image response and the parameter estimation problem for
closely spaced optical targets. In this section we will present
some computer results regarding the Cramer-Rao bounds and degrada-
tion factors for the target intensity and angular position estimation.
These quantities were computed according to (3.8), (4.8), (4.11),
(4.13), (4.14), (4.25) and (4.26) with respect to three parameters:
β (the detector size along the scanning direction normalized by
the optical resolution λ/d), $\alpha\Delta\tau$ (the angular separation between
two targets normalized by λ/d) and N_e (the detected electron counts
due to background noise during the integration interval when the
detector width is equal to λ/d).

In the previous discussions we considered the target positions
as points on the time axis. However, in the real computation, for
convenience, we considered them in terms of angles normalized by
λ/d. These two measures are different only by a constant, α, the
normalized linear scan rate. The degradation factor for the position
estimate remains the same no matter which quantity is used to
measure target position. However, the CRB for the angular position
estimate, CRB ($\alpha\tau,n$), becomes the product of α^2 and the CRB for the
time position estimate, CRB (τ,n), which was defined earlier in
Section IV.

The ranges for β and $\alpha\Delta\tau$ employed in the computation were $.2 \leq \beta \leq 5$ and $.1 \leq \alpha\Delta\tau < 2$, respectively. An arbitrary value, 100, was used for N_e. The samples used in all computations were equally spaced in the range of $\alpha\tau$ from -6.4 to 6.4 at an interval of .05. For all values of β and $\alpha\Delta\tau$ considered here, this range is large enough to cover the important portion of the associated optical signal and the sampling frequency is well above the Nyquist frequency.

Fig. 3 shows a set of DF_a curves as functions of β and $\alpha\Delta\tau$ for the case where $\tilde{a}_1 = \tilde{a}_2 = .01$ and $N_e = 100$. Fig. 4 shows the DF_τ curves for the same condition. From these figures it is obvious that as $\alpha\Delta\tau$ becomes larger both DF_a and DF_τ become smaller and asymptotically converge to unity. This implies that when the interfering target is angularly further apart from the desired target, it can do less impairment to the estimation of target intensity and location and hence the estimates should be more reliable. From Fig. 3, we also see that, at any target separation, the degradation factor for intensity estimate is always smaller for a detector with smaller detector width. However, it is not entirely true for the degradation factor of the position estimate as shown in Fig. 4 where the degradation factor for $\beta=5$ is smaller than that for $\beta=2$ when the angular separation is approximately over .8 λ/d.

Figs. 5 and 6 show an example of how the degradation factors vary with different intensities of the interfering target in the simple shot-noise limited case. In this example, $\tilde{a}_1=1$, $N_e=100$

and $\tilde{a}_2$ is chosen as .1, 1, 10 and 100. From these figures it is
clear that at any angular separation both degradation factors be-
come larger for stronger interference. This means that the stronger
the interfering target, the more severe is its influence on the in-
tensity and position estimation of the desired target. Note that
the ordinates in Figs. 5 and 6 can be also used to indicate
$\sqrt{CRB(\tilde{a}_1, n=2)}/\tilde{a}_1$ (lower bound on normalized standard deviation of
intensity estimates) and $\sqrt{CRB(\alpha\tau_1, n=2)}$ (lower bound on standard
deviation of angular position estimates normalized by λ/d) respect-
ively. For examples, when $\tilde{a}_1=\tilde{a}_2=\beta=1$ they are 2.65% and .016 for
$\alpha\Delta\tau=1$ respectively.

Fig. 7 shows the degradation factors of intensity estimation
for several pairs of $\tilde{a}_1$ and $\tilde{a}_2$. The detector size used is $\beta=1$.
We can see that in the background-noise limited cases where $\tilde{a}_1 << \beta$
and $\tilde{a}_2 << \beta$ the degradation factor becomes independent of a_1's.
However, this particular relationship does not arise for other cases
where $\tilde{a}_1$ is comparable or much greater than β, as indicated by
curves for $\tilde{a}_1=\tilde{a}_2=1$, $\tilde{a}_1=\tilde{a}_2=10$ and $\tilde{a}_1=\tilde{a}_2=100$. The same conclusion
applies for the degradation factors of location estimation although
they are not shown. This figure should clarify the assertion made
in section 4.2.

The conditions in Figs. 3 and 4 can be considered as being
background-noise limited because $\tilde{a}_1$ is much smaller than all β's
considered. Since the degradation factors for the background-noise
limited case are independent of the target intensity as illustrated
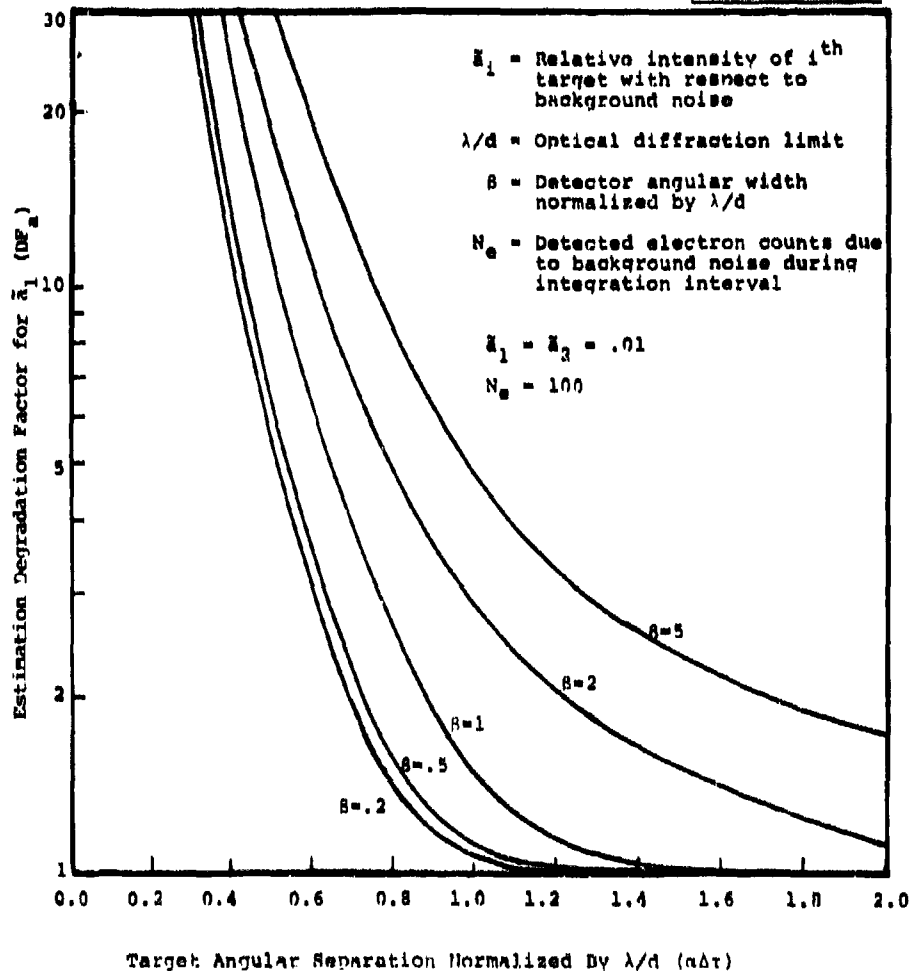
31

Fig.3. Degradation of intensity estimation of the first target due to interference of the second target computed for different detector sizes and angular separations; a background noise limited case.
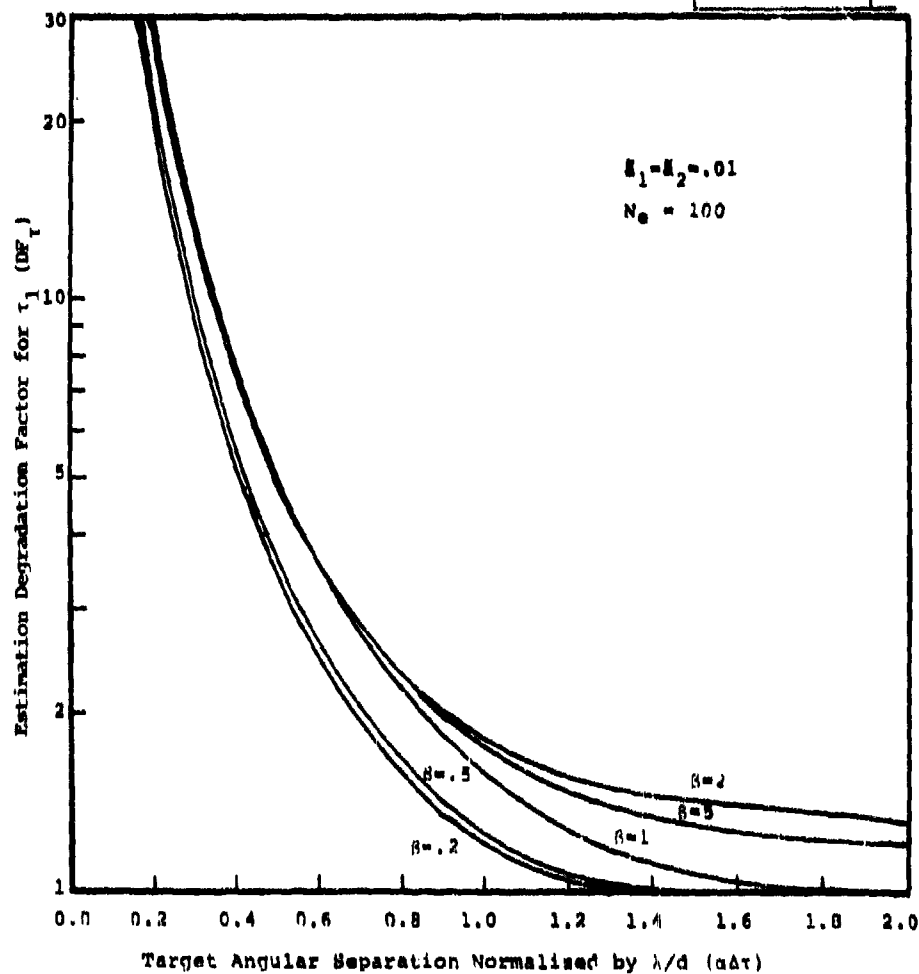
Fig.4. Degradation of angular position estimation of the first target due to interference of the second target computed for different detector sizes and angular separations; a background noise limited case.

by Fig. 7, the degradation curves shown in Figs. 3 and 4 are the limiting curves for all background-noise limited cases. Figs. 5 and 6 which show the effect of interference can also serve to demonstrate the signal-dependence of degradation factors.

Figs. 8 and 9 show the CRB curves as functions of β and $\alpha\Delta\tau$ for $\tilde{a}_1 = 10$, $\tilde{a}_2 = 1$ and $N_e = 100$. Scales for $CRB^{\frac{1}{2}}(\tilde{a}_1, n=2)/\tilde{a}_1$ and $CRB^{\frac{1}{2}}(\alpha\tau_1, n=2)$ are also provided. As expected, the CRB on either the intensity or position estimate decreases as the angular separation increases for all detector sizes. However, no distinct relationship between the detector size and its associated Cramer-Rao bound can be observed from these figures. For this particular example, it can be observed that the detector size which yields the lowest CRB is different for different ranges of target separation. This result may be due to the particular detector response function assumed which was discussed in [5], or the fact that detectors with smaller (larger) size can increase (decrease) the resolution capability but, on the other hand, can also decrease (increase) the device sensitivity.

Fig. 10 illustrates the relationship between the signal-to-noise ratio (dB), target intensities and target separation. The SNR_t^1 is computed at $t = \tau_1$ according to Eq. (4.24). This figure illustrates that the signal-to-noise ratio decreases significantly when the interfering target is stronger than and/or close to the desired target. The additional noise power due to the interfering target fades out, as one expects, while the target separation is large. This is demonstrated by the fact that all curves tend to
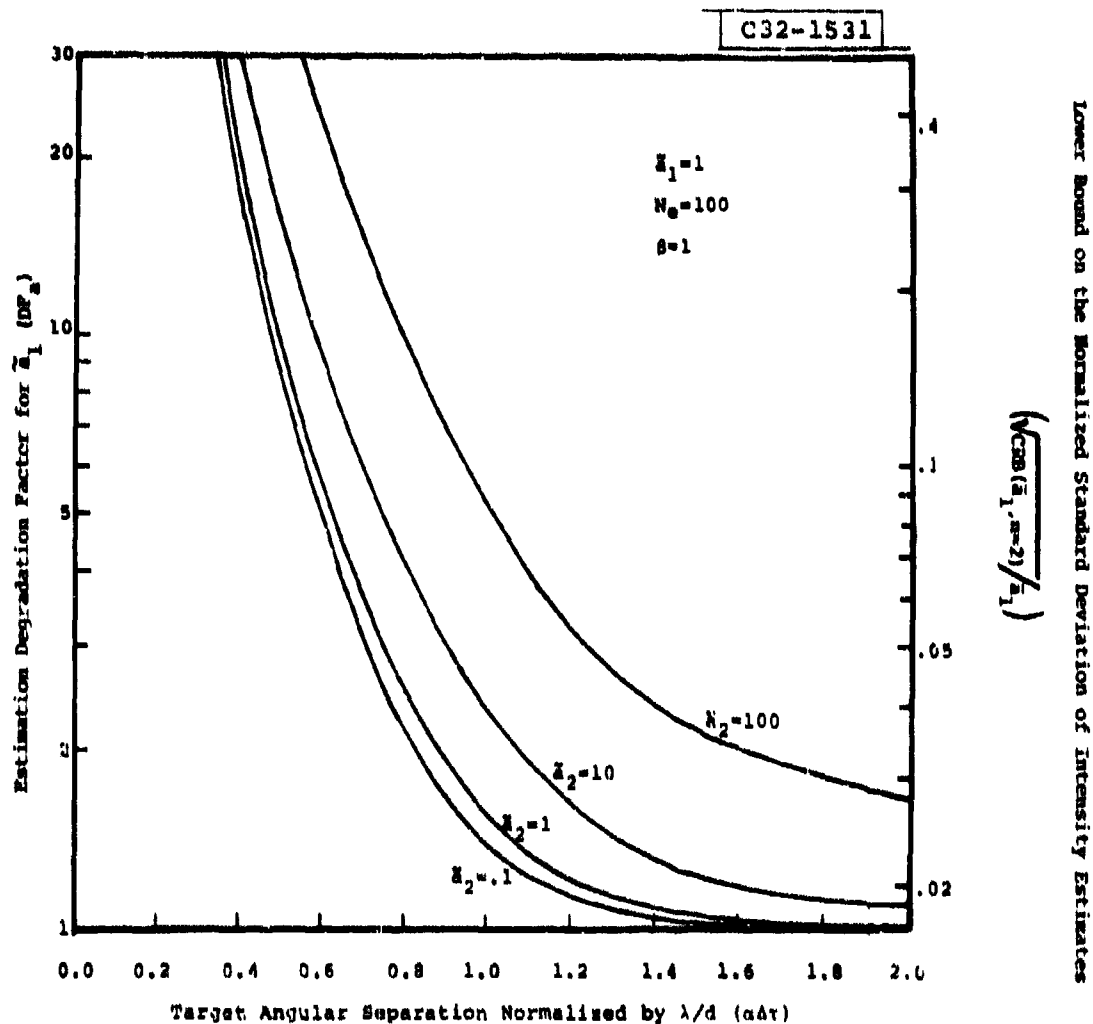
34

Fig.5. Effect of different intensities of the second
target on the degradation factor of intensity estimation
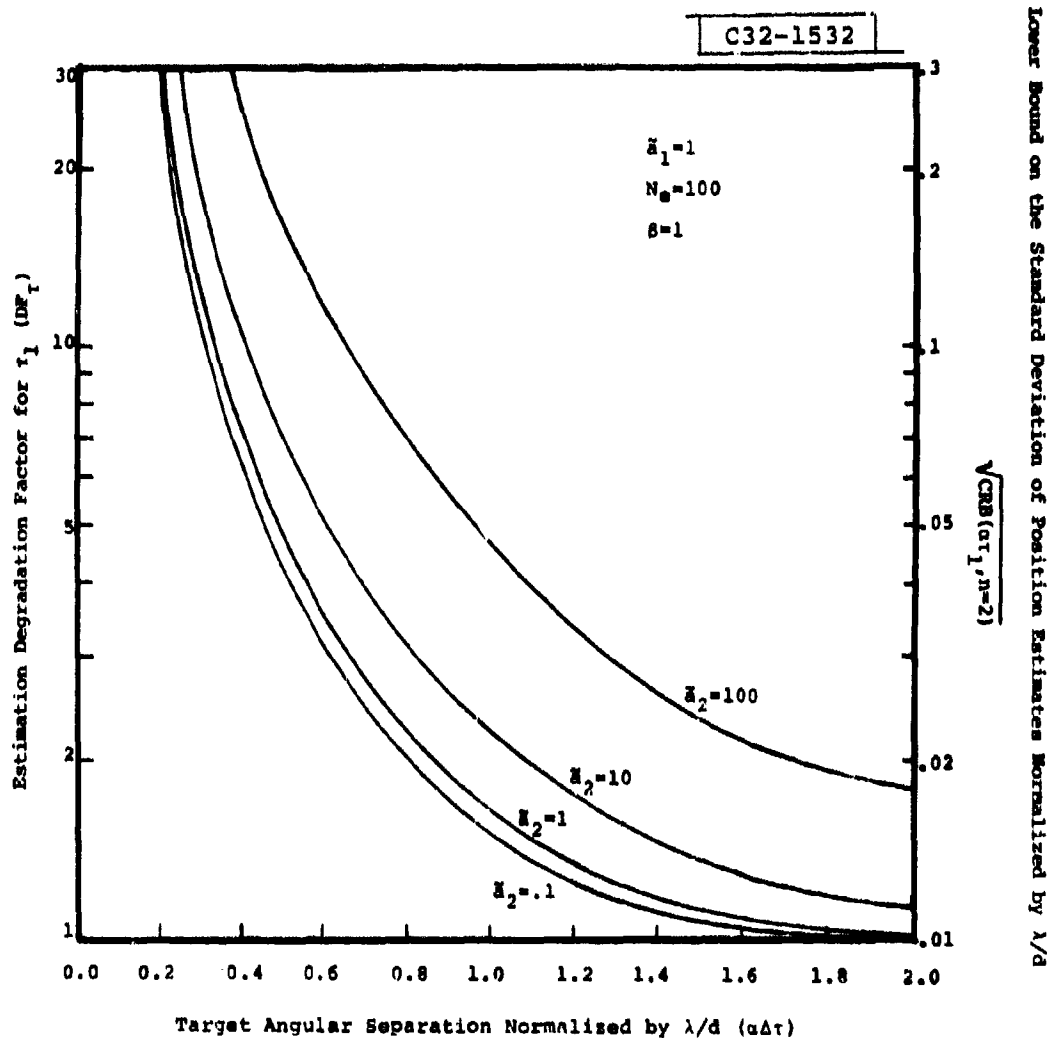of the first target; a sample example.

Fig.6. Effect of different intensities of the second target on the degradation factor of position estimation of the first target; a sample example.
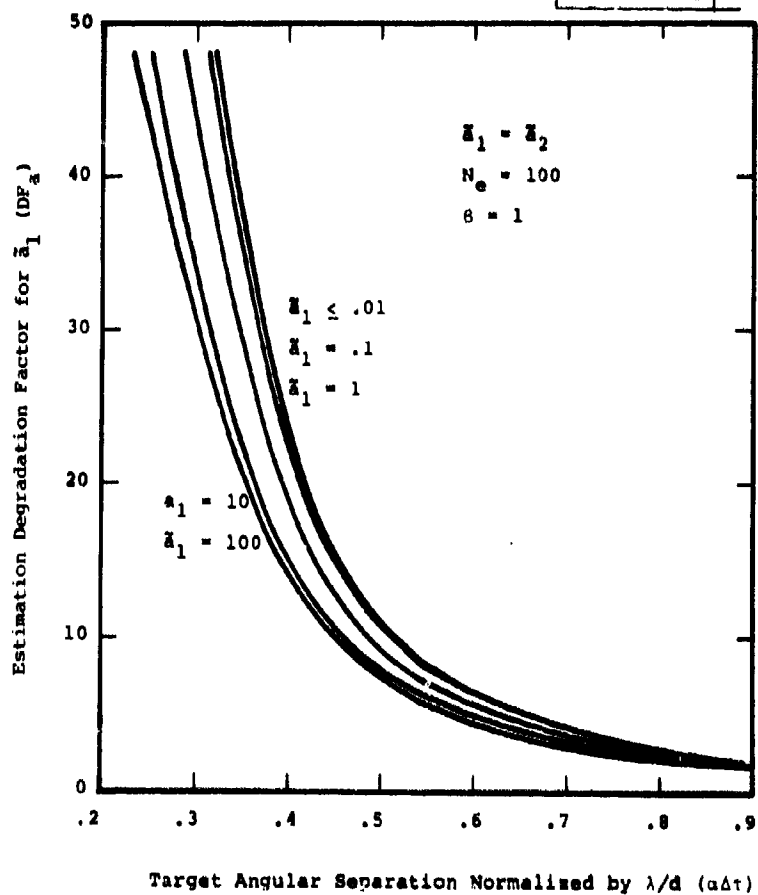
Fig.7. Degradation factors of intensity estimation for a wide range of target intensity.
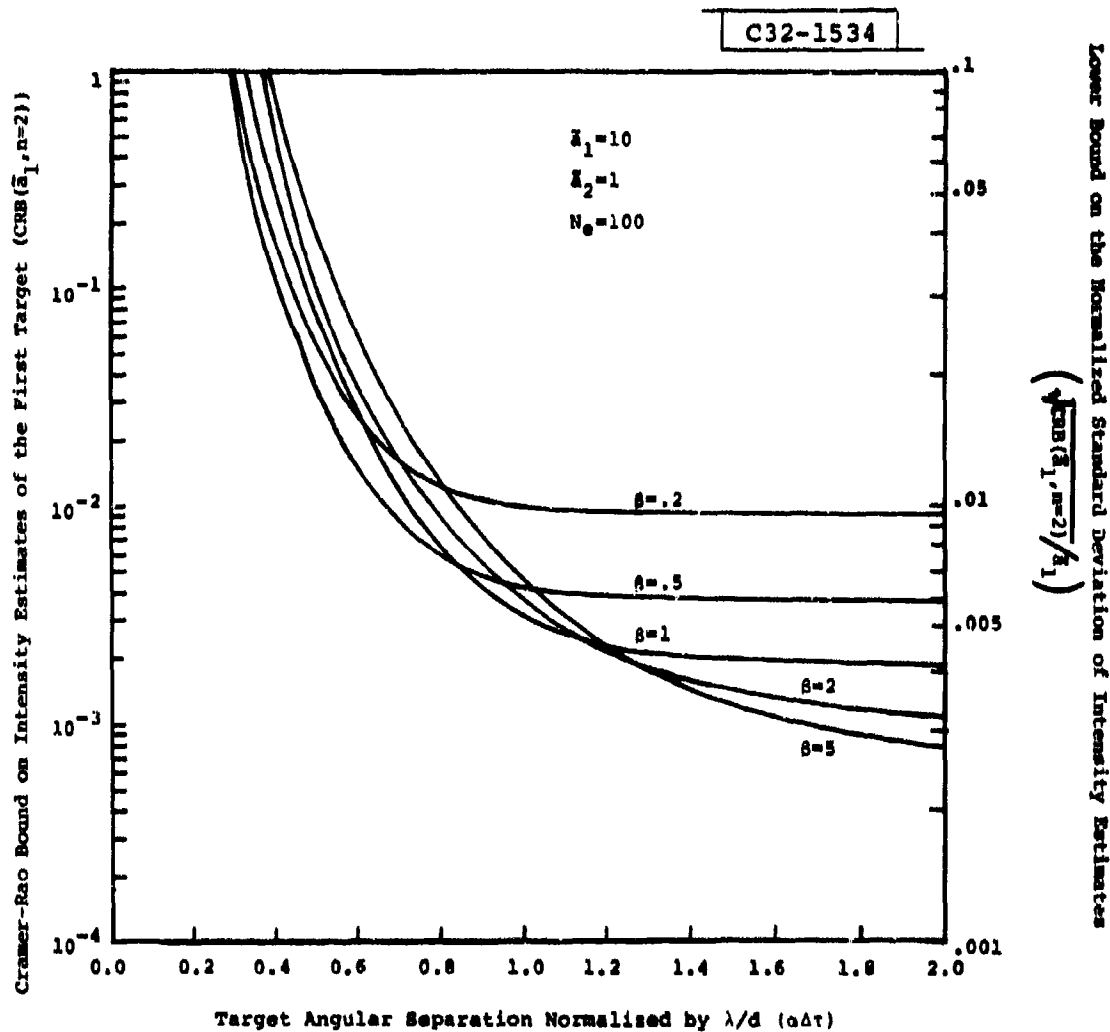
Fig. 8.   The Cramer-Rao bound of intensity estimate of
the first target computed for different detector sizes
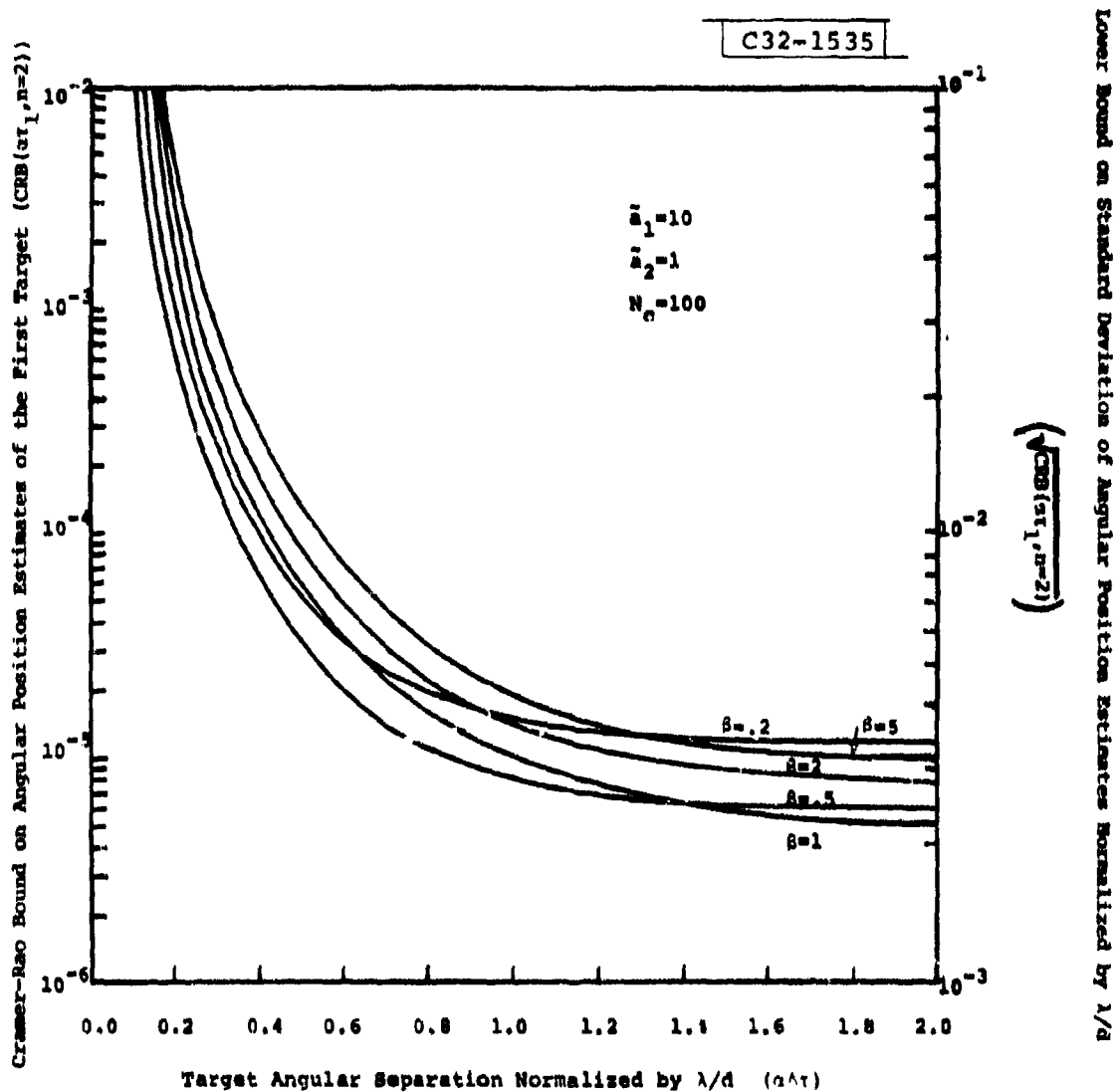and angular separations; a shot-noise limited case.

Fig.9. The Cramer-Rao bound of angular position estimate of the first target computed for different sizes and angular separations; a shot-noise limited case.
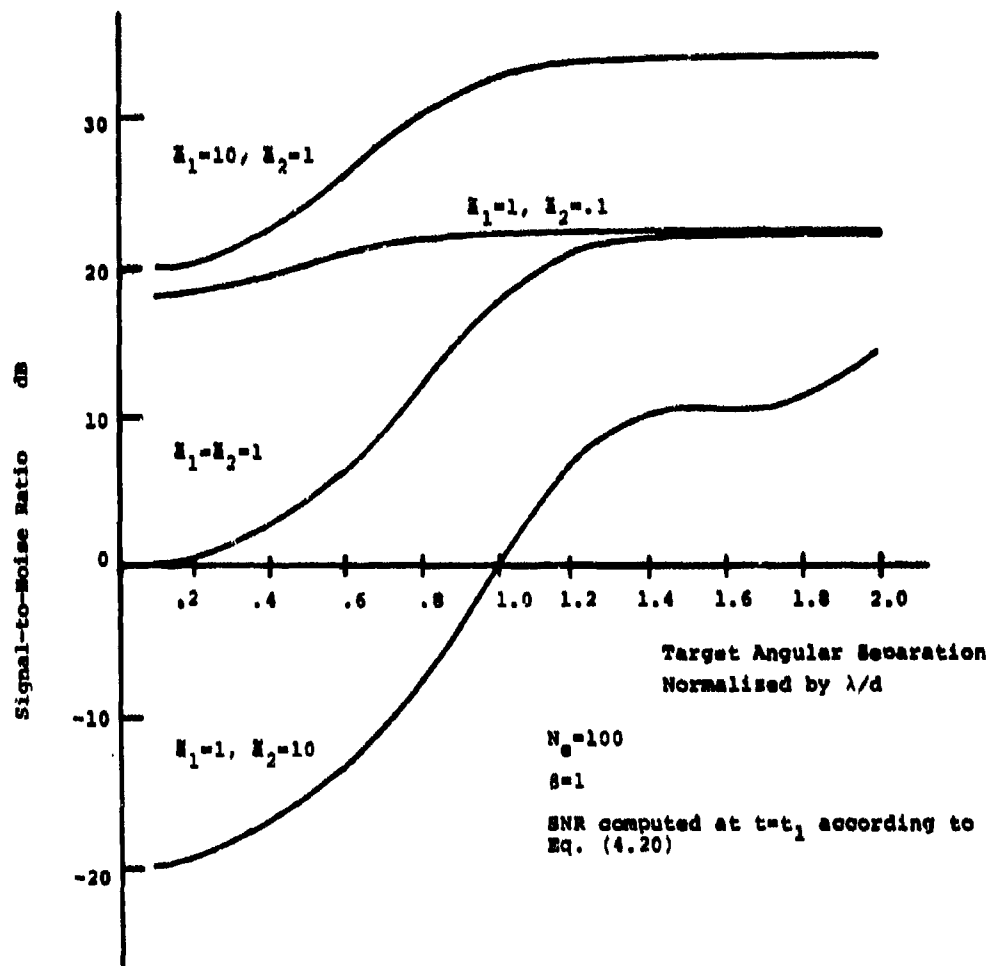
39

Fig.10. The relationship between signal-to-noise ratio
(SNR), targets relative intensities ($\tilde{a}_1, \tilde{a}_2$) and the
separation between the targets ($\alpha\Delta\tau = \Delta\theta/(\lambda/d)$).

level off asymptotically. Comparing Fig. 10 with Figs. 5, 6, 8 and 9 we can see that the estimation performance varies monotonically with signal-to-noise ratio. It should be noted that the oscillation shown in the bottom curve of Fig. 10 is due to the sidelobes of the optical pulse shape assumed in Section III.

Figs. 11 and 12 show the estimation accuracy in the case of a single target in relation to the normalized target intensity, $\tilde{a}_1$, and the detected electron counts due to the uniform background radiation, N_e. The detector angular width is choosen equal to λ/d. It is clear that for a fixed value of N_e the estimation accuracy of intensity estimation, expressed by $CRB(\tilde{a}_1, n=1)/\tilde{a}_1$, and that of angular position estimation, expressed by $CRB(\alpha\tau_1, n=1)$, decrease monotonically as $\tilde{a}_1$ increases. In fact, the decrease is linear in log-log scale with slope equal to 1 for the background-noise limited case($a_1 << \beta$) and with slope equal to $\frac{1}{2}$ for the quantum limited case ($\tilde{a}_1 >> \beta$). This difference is attributed to the characteristics of the shot-noise in which the noise is dependent upon the signal in addition to the background noise. The stronger the target the more noise is generated and the increase in noise level effectively off-sets some advantage gained with stronger signal.

From Figs. 11 and 12 it also can be seen that for the same $\tilde{a}_1$ the estimation accuracy is inversely proportional the square root of N_e. Note that N_e is equal to $\sigma\tau_p P_{bo}$ as defined in (4.15) and $\tilde{a}_1$ is the intensity relative to P_{bo}. The actual value of N_e could vary in a wide range depending upon the background condition and the
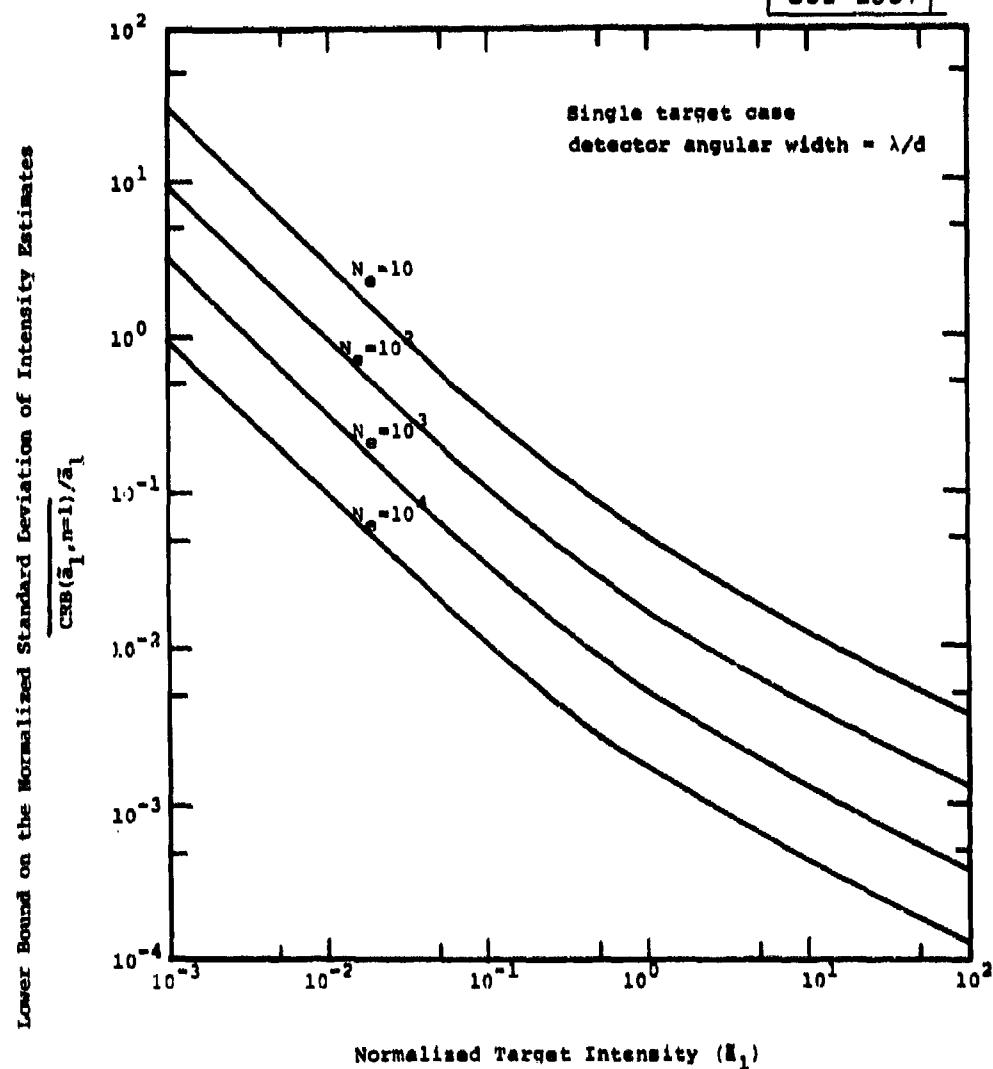
41

Fig.11. Accuracy of intensity estimation in the case of a single target in relation to the normalized target intensity ($\tilde{a}_1$) and the detected electron counts due to background radiation (N_e).

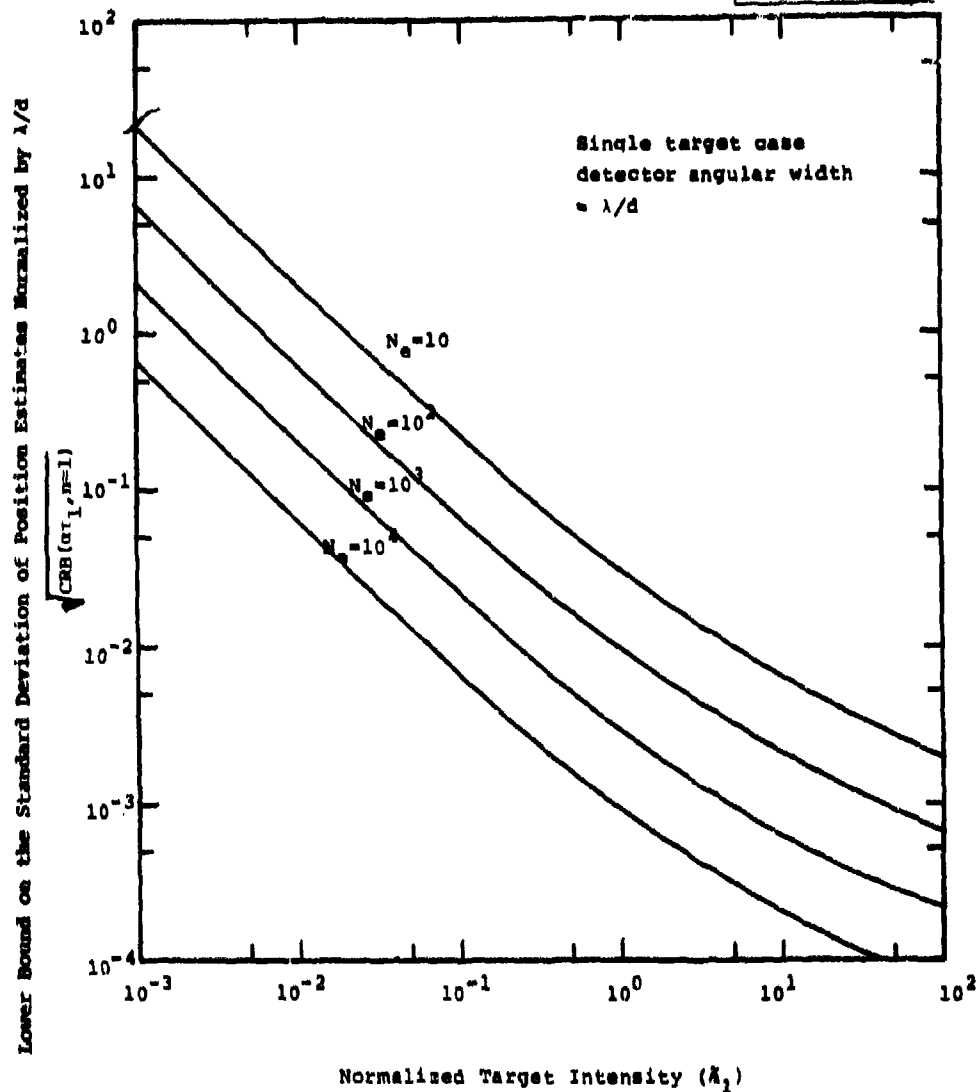Fig.12. Accuracy of angular location estimation in the case of a single target in relation to the normalized target intensity ($\tilde{a}_1$) and the detected electron counts due to background radiation (N_e).

43

particular sensor system used. If ρ and τ_p are constant then for an absolute target intensity, a_1, the corresponding $\tilde{a}_1$ is different for different N_e. Therefore when figures which are shown in terms of relative quantities are used to interpret the absolute physical measurements care should be exercised.

It is worthwhile to note that Figs. 11 and 12 can be coupled with the degradation factor curves (e.g., those shown in Figs. 3 and 4) to give the actual estimation accuracy of the desired target in the presence of an interfering target. On the other hand these figures can also be coupled with the estimation accuracy curves (e.g., those shown in Figs. 8 and 9) to yield the estimation degradation factors.

VI.   CONCLUSIONS

In this report we have presented a mathematical model for
passive optical detectors and the Cramer-Rao bounds on the var-
iances of intensity and angular location estimates of two closely
spaced optical targets. We have emphasized the case in which the
system is shot noise (not background noise) limited. Representative
curves for the Cramer-Rao bounds and the performance degradation
factors are shown.

An intrinsic noise source for the passive optical estimation
system arises from Poisson shot noise. The mean signal in the shot-
noise current is proportional to the input signal. However, the
variance of the shot noise current is also dependent upon the sig-
nal in addition to any background radiation noise.

Owing to the nature of the shot noise and the presence of a
second target, the estimation of the first target's intensity and
angular location is a complicated procedure. It is found that the
estimation performance degrades as the separation between the two
targets becomes small and that there is no clear implication from
the values of the lower bounds that there is an optimal selection
of detector size.

It should be noted that the Cramer-Rao bounds derived for two
target cases in this report implicitly assume that the two targets
have been "resolved". We did not address the CSO resolution problem
completely in this report. We feel that the combined detection and

estimation problem must be addressed in order to provide a more balanced view of the resolution problem. We must also alert the readers to the fact that the Cramer-Rao lower bounds are theoretical limitations for unbiased estimators. An estimation algorithm which is combined with certain detections schemes may become a _biased_ estimator even if the estimator alone is unbiased in the absense of a detection procedure. In order to answer questions about how close can one resolve two adjacent targets, it may be necessary to carry out Monte Carlo simulations. It is expected that the simulation results will be heavily dependent upon the specific algorithms one chooses.

This report does not include the comparison between our result and results in references [3]-[5] which assumed different image diffraction patterns and different noise conditons. A Monte Carlo simulation study for a specific algorithm is also deferred. These will be the subjects of subsequent reports.

46

ACKNOWLEDGMENTS

47

REFERENCES

1. J. R. Sklar and F. C. Schwepee, "On the Angular Resolution of Multiple Targets," Proc. IEEE, 52, 1044 (1964).

2. G. E. Pollon and G. W. Lank, "Angular Tracking of Two Closely Spaced Radar Targets," IEEE Trans. Aerospace Electron Systems, AES-4, 541 (1968).

3. D. L. Fried, "Resolution, Signal-to-Noise Ratio and Measurement Precision," Optical Science Consultants, Report No. TR-034, (October, 1971).

4. R. W. Miller, "Accuracy of Parameter Estimates for Unresolved Objects," Technical Note 1978-20, Lincoln Laboratory, M.I.T. (8 June 1970), DDC AD-B028168.

5. R. W. Miller, private communications.

6. R. M. Gagliardi and S. Karp, Optical Communications, (Wiley, New York, 1976).

7. D. L. Snyder, Random Point Processes, (Wiley, New York, 1975).

8. E. Parzen, Stochastic Porcesses, (Holden-Day, San Francisco, 1962).

9. M. Born and E. Wolf, Principles of Optics, (MacMillan, New York, 1964).

10. K. Seyrafi, "Electro-Optical Systems Analysis," Electro-Optical Research Company, Los Angeles, (1973).

11. H. L. Van Trees, Detection, Estimation, and Modulation Theory, Vol. I (Wiley, New York, 1971).

12. H. L. Van Trees, Detection, Estimation, and Modulation Theory, Vol. III (Wiley, New York, 1968).

13. C. W. Helstrom, Statistical Theory of Signal Detection, 2nd Edition (Pergamon Press, New York, 1968).

14. L. P. Seidman, "Performance Limitations and Error Calculations for Parameter Estimation," Proc. IEEE 58, 644 (1970).

REPORT DOCUMENTATION PAGE		READ INSTRUCTIONS BEFORE COMPLETING FORM
1. REPORT NUMBER ESD-TR-79-151	2. GOVT ACCESSION NO.	3. RECIPIENT'S CATALOG NUMBER
4. TITLE (and Subtitle) Performance Limitations on Parameter Estimation of Closely Spaced Optical Targets Using Shot-Noise Detector Model		5. TYPE OF REPORT & PERIOD COVERED Technical Note
		6. PERFORMING ORG. REPORT NUMBER Technical Note 1979-35
7. AUTHOR(s) Ming-Jer Tsai and Keh-Ping Dunn		8. CONTRACT OR GRANT NUMBER(s) F19628-78-C-0002
9. PERFORMING ORGANIZATION NAME AND ADDRESS Lincoln Laboratory, M.I.T. P.O. Box 73 Lexington, MA 02173		10. PROGRAM ELEMENT, PROJECT, TASK AREA & WORK UNIT NUMBERS Project No. 8X363304D215
11. CONTROLLING OFFICE NAME AND ADDRESS Ballistic Missile Defense Program Office Department of the Army 5001 Eisenhower Avenue Alexandria, VA 22333		12. REPORT DATE 13 June 1979
		13. NUMBER OF PAGES 56
14. MONITORING AGENCY NAME & ADDRESS (if different from Controlling Office) Electronic Systems Division Hanscom AFB Bedford, MA 01731		15. SECURITY CLASS. (of this report) Unclassified
		15a. DECLASSIFICATION DOWNGRADING SCHEDULE

16. DISTRIBUTION STATEMENT (of this Report)

Approved for public release; distribution unlimited.

17. DISTRIBUTION STATEMENT (of the abstract entered in Block 20, if different from Report)

18. SUPPLEMENTARY NOTES

None

19. KEY WORDS (Continue on reverse side if necessary and identify by block number)

passive optical sensors	Cramer-Rao bound	parameter estimation
shot-noise process	degradation	closely spaced objects
detector model		

20. ABSTRACT (Continue on reverse side if necessary and identify by block number)

A mathematical model for passive optical sensors, which takes into account the inherent shot-noise process, is presented. Based on this sensor model, the Cramer-Rao bounds on the variances of intensity and angular location estimates for two closely spaced optical targets are derived. Representative results for the estimation performance degradation due to the interfering targets are shown.

DD FORM 1473 EDITION OF 1 NOV 65 IS OBSOLETE
1 JAN 73